PERGAMON

Chemical Engineering Science 57 (2002) 805–820

Chemical Engineering Science

www.elsevier.com/locate/ces

Mathematical modeling of an in-line low-NO_x calciner

I. Iliuta[a,1], K. Dam-Johansen[a,*], L. S. Jensen[b]

[a] *Department of Chemical Engineering, Technical University of Denmark, Building 229, DK-2800 Lyngby, Denmark*
[b] *F.L. Smidth & Co. A/S, Vigerslev Alle 77, DK-2500 Valby, Copenhagen, Denmark*

Received 14 November 2000; received in revised form 4 May 2001; accepted 27 October 2001

Abstract

The reduction of the NO_x content in in-line-calciner-type kiln systems can be made by optimization of the primary firing in the rotary kiln and of the secondary firing in the calciner. Because the optimization of calciner offers greater opportunities the mathematical modeling of this reactor is very important. A heterogeneous, dynamic mathematical model for an in-line low-NO_x calciner based on non-isothermal diffusion–reaction models for char combustion and limestone calcination has been developed. The importance of the rate at which preheated combustion air was mixed into the main flow was particularly studied. The results of the simulations indicate that the external heat and mass transfer to the char particles is not limiting. Internal diffusion of O_2, CO, NO and CO_2 is important especially in the reducing zone and the first part of the oxidizing zone of the calciner and the internal heat transport limitation is significant for the endothermic limestone calcination. The rate at which preheated combustion air is mixed into the main flow directly influences the coal combustion rate, and thereby through the rate of heat release from combustion, it also influences the calcination rate and the temperature profile. The mixing rate has some influence on the CO concentration profile and an important influence on the overall degree of fuel-N to NO conversion.

Keywords: Cement production; Calciner; Combustion; Calcination; Modeling

1. Introduction

Cement production involves the thermal conversion of a raw meal consisting of approximately 75–80% $CaCO_3$ into clinker (Andersen, 1981). Raw meal is produced by finely grinding and homogenizing the raw materials. It is subsequently preheated by heat exchange with the hot process gases, then calcined, converted to clinker, cooled by heat exchange with cold combustion air and finally ground with gypsum to form cement. The pyroprocessing operations typically take place in a kiln system, which comprises a preheater, a calciner, a rotary kiln and a clinker cooler. Calcination of $CaCO_3$ is strongly endothermic and the most energy demanding reaction. Typically, this energy requirement is met by firing about 1900 kJ fuel/kg produced clinker in a calciner operated in the temperature range 830–1200°C. Clinker formation typically takes place in a rotary kiln where a further 1300 kJ fuel is burned per kg produced clinker. The most commonly employed fuels for cement production are pulverized coal or petcoke.

Large fuel consumption results in cement production having a significant emission potential for combustion generated pollutants, of which NO_x is a major concern. NO_x is primarily formed at two positions in kiln systems for cement clinker production: in the rotary kiln and calciner. In the rotary kiln, NO_x is formed both from atmospheric N_2 and from fuel bound N, whereas NO_x only can be formed from fuel-bound N in the calciner because of the low operating temperatures. Due to the high clinkering temperature, it is difficult to significantly reduce NO_x formation in the rotary kiln. Primary measures for reducing NO_x formation have therefore mainly been focused at optimizing calciner design with respect to controlling NO_x emissions. Focus has particularly been on in-line-calciner-type kiln systems, where the flue gas from the rotary kiln passes through the calciner. This is because this kiln system type allows NO_x from the rotary kiln to react with the fuel fired in the calciner, and thereby be partly reduced to N_2 (Jensen, 1999).

Several in-line-type low-NO_x calciner designs have been developed by machinery suppliers to the cement industry. This modeling work is concerned with the F. L. Smidth

* Corresponding author. Tel.: +45-45252800; fax: +45-45252845.
E-mail address: kdj@kt.dtu.dk (K. Dam-Johansen).
[1] On leave from Department of Chemical Engineering, University *Politehnica* of Bucharest, Polizu 1, 78126 Bucharest, Romania.

0009-2509/02/$ - see front matter
PII: S0009-2509(01)00420-1

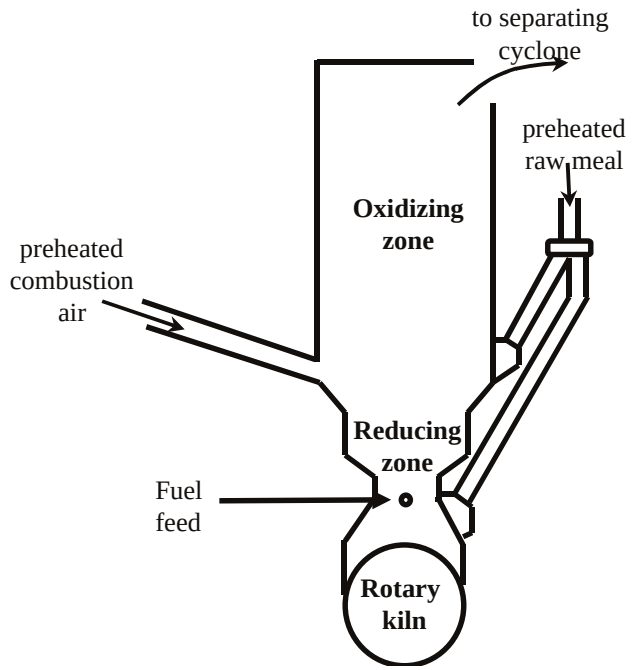

Fig. 1. Illustration of an in-line low-NO_x calciner (from Thomsen et al., 1998).

in-line low-NO_x calciner (ILC), and this is therefore the calciner type described in the following. Fig. 1 schematically shows the in-line low-NO_x calciner design (Thomsen, Jensen, & Schomburg, 1998). Flue gas from the rotary kiln enters the calciner through the bottom, where all of the calciner fuel is fed in the reducing zone together with a fraction of the preheated raw meal, which is added to control the temperature. After a mean gas residence time of approximately 0.2 s, all of the combustion air and the remaining raw meal is added. The suspension subsequently passes up through the oxidizing zone of the calciner, wherefrom it, after a gas residence time of approximately 3–4 s, proceeds into a cyclone separating the solid from the gas phase.

In calciners, the NO_x emission is the result of competition between NO_x formation (from volatile-N, char and tar) and NO_x reduction. The main factors influencing formation and reduction of NO are physical and chemical properties of the fuel (volatile matter and initial carbon contents) and operating conditions (temperature, presence of CO and oxygen, NO concentration). Control of NO_x emissions requires both optimization of combustion in the rotary kiln and calciner (Jeschar, Jennes, Kremer, & Kellerhoff, 1996). Because of the limited possibilities for reducing NO_x formation in the rotary kiln, there is a much greater focus on optimizing calciner design due to its greater potential for NO_x emission control. Mathematical modeling of calciners is a valuable tool for optimizing calciner design because it facilitates a simultaneous analysis of the large number of simultaneously proceeding chemical reactions and physical processes.

Despite the numerous laboratory studies of reaction kinetics and mechanisms that are being released in the academic and patent literature, there are few attempts in the field of modeling calciners. Scheuer (1987), Jeschar et al. (1996) and Jeschar, Jennes, Kremer, and Kellerhoff (1999) developed so-called homogeneous mathematical models for the calciner. A major lack of these models is that they do not include the heterogeneous gas–char reactions, tar combustion, heterogeneous catalyzed reactions and hydrocarbon radical reactions. Char is the main pyrolysis product of the most commonly employed fuels in calciners (coal and petcoke) and contains the majority of nitrogen. This makes char-N the greatest potential NO_x source. Also, the tar is a major product of bituminous coal pyrolysis and it may also contain a significant fraction of fuel-N. Jensen (1999) developed a homogeneous model for an in-line low-NO_x calciner including pseudo-reactions for char and tar, and gradual mixing after the introduction of the combustion air. The flow model consists of two plug-flow reactors—one representing the reducing zone and the other representing the oxidizing zone above the last combustion air inlet. Mixing of combustion air in oxidizing zone was modeled using a modified Zwietering approach, which supposes that combustion air is gradually mixed into the main flow. Coal pyrolysis was assumed to be instantaneous, homogeneous gas phase reactions were described by the comprehensive kinetic model of Glarborg, Alzueta, Dam-Johansen, and Miller (1998), heterogeneous char–gas reactions was described by lumped kinetic parameters and the reactions of the tar were described in an empirical manner.

None of the above models takes the coupling between the coal particle combustion and limestone particle calcination into account. This is complicated and depends on the inter-phase and intra-particle heat and mass transport, kinetics, thermodynamics, flow patterns and hydrodynamics.

The major objective of this paper is to develop a heterogeneous mathematical model for an in-line low-NO_x calciner based on non-isothermal diffusion–reaction models for char combustion and limestone calcination. Model results are then compared with measurements on a full-scale in-line low-NO_x calciner.

2. Mathematical model development

The in-line low-NO_x calciner model consists of an axial dispersion flow model for gas and solid phases coupled with the non-isothermal diffusion–reaction models for char combustion and limestone calcination, homogeneous gas phase reactions, heterogeneous catalyzed and combustion reactions: all influenced by gradual mixing of air into the reactor. Pyrolysis of the coal was assumed instantaneous. Mixing in the oxidizing zone is modeled using a modified Zwietering approach, which supposes that combustion air is gradually mixed into the main flow. Solid holdup was calculated using the model developed by Nieuwland, Delnoij, Kuipers, and van Swaaij (1997).

2.1. Physical model of the calciner

Reducing zone. In the bottom of the reducing zone, a fraction of the preheated raw meal and all the coal are admitted into the rotary kiln flue gas (Fig. 1). In the reducing zone, the following processes take place simultaneously: mixing of coal and raw meal into the main flow, transport of gaseous and solid components up through the reducing zone, pyrolysis of coal and reactions of pyrolysis products, char combustion and NO formation/destruction and heating and calcination of limestone. As a first model approximation, an axial dispersion model was used to describe the gas and solid flow (Wei, Lin, & Yang, 1993; Namkung & Kim, 1998). Mixing and coal pyrolysis were assumed instantaneous. The composition of the pyrolysis gas was approximated as a mixture of H_2, NH_3, H_2O, C_3H_8, C_2H_4, CH_4, CO and CO_2 based on the pyrolysis gas composition from a bituminous coal determined by Greul, Rüdiger, Spliethoff, and Hein (1993), and the reducing zone was assumed operated under adiabatic conditions. Char and limestone particles were considered non-isothermal and the external resistance to heat transfer was taken into account.

Oxidizing zone. In the bottom of the oxidizing zone, the sub-stoichiometric suspension flowing up from the reducing zone is mixed with combustion air and the remaining fraction of the preheated raw meal. As oxygen from combustion air is mixed into the flow, combustion takes place thereby releasing heat. This heat is transferred to the calcining limestone contained in the raw meal. If the heat release from combustion is more rapid than the rate of heat consumption by calcination, the temperature rises. In the oxidizing zone, the following processes take place simultaneously: mixing of combustion air and raw meal into the main flow, transport of gaseous and solid components up through the oxidizing zone, char combustion, NO formation and destruction, heating and calcination of limestone, homogeneous gas phase reactions and heterogeneous gas–solid and catalytic reactions. As employed for the reducing zone, an axial dispersion model was also used to describe the gas and solid flow in the oxidizing zone (Wei et al., 1993; Namkung & Kim, 1998). The oxidizing zone was assumed operated under adiabatic conditions and the char and limestone particles were considered non-isothermal. Mixing in the oxidizing zone was modeled using a modified Zwietering approach, which supposes that combustion air is gradually mixed into the main flow.

2.2. Char combustion and NO formation/destruction sub-models

2.2.1. Reaction network

The model of char combustion couples the heterogeneous reactions of char with oxygen and carbon dioxide within the porous particles to the homogeneous oxidation of CO (Table 1). Each char particle was assumed non-isothermal.

Table 1
Heterogeneous and homogeneous reactions for char combustion and NO formation/destruction

Reaction	
(1)	$C + \frac{\alpha+2\beta}{2(\alpha+\beta)}O_2 \overset{r_{oxdn}}{\rightarrow} \frac{\alpha}{\alpha+\beta}CO + \frac{\beta}{\alpha+\beta}CO_2$
(2)	$C + CO_2 \overset{r_{gasn}}{\rightarrow} 2CO$
(3)	$CO + \frac{1}{2}O_2 \overset{r_{co}}{\rightarrow} CO_2$
(4)	$Char - N + \frac{1}{2}O_2 \overset{r_{form}}{\rightarrow} NO$
(5)	$C + NO \overset{r_{dest}}{\rightarrow} CO + \frac{1}{2}N_2$

The oxidation reaction was assumed to follow a Langmuir–Hinshelwood–Hougen–Watson kinetics. The volumetric (per unit particle volume) intrinsic carbon consumption rate with oxygen was taken as (Lewis & Simons, 1979):

$$r_{oxdn} = \frac{k_1 k_2 P_{O_2}}{k_2 + k_1' + k_1 P_{O_2}} a_{ch}, \tag{1}$$

$$k_1 = 7.41 \times 10^{-3} \exp(-19,000/T),\ \text{kmol/m}^2\ \text{s Pa}, \tag{1a}$$

$$k_2 = 75.0 \exp(-19,000/T),\ \text{kmol/m}^2\ \text{s}, \tag{1b}$$

$$k_1' = 1.67 \times 10^2 k_1 k_2 \exp(-3500/T),\ \text{kmol/m}^2\ \text{s}, \tag{1c}$$

where k_1 is the adsorption coefficient for oxygen, k_1' is the desorption coefficient for oxygen and k_2 is the desorption coefficient for reaction product.

The CO_2–char gasification reaction (reaction 2, Table 1) was also assumed to follow Langmuir kinetics. The volumetric intrinsic carbon consumption rate with carbon dioxide has been taken as (Ballal & Zygourakis, 1986):

$$r_{gasn} = \frac{k_3 P_{CO_2}}{1 + k_4 P_{CO_2} + k_5 P_{CO}} a_{ch}, \tag{2}$$

where

$$k_3 = 2.02 \times 10^{-3} \exp(-30,905/T), \quad \text{kmol/m}^2\ \text{s Pa}, \tag{2a}$$

$$k_4 = 3.75 \times 10^{-10} \exp(301/T),\ 1/\text{Pa}, \tag{2b}$$

$$k_5 = 1.05 \times 10^{-7} \exp(-5729/T),\ 1/\text{Pa}. \tag{2c}$$

The H_2O–char gasification reaction was neglected (char consumption within a system containing low levels of moisture primarily proceeds by the two gas–solid reaction mentioned (Laurendeau, 1978).

Homogeneous oxidation of carbon monoxide was assumed to take place only in the bulk gas phase and not in the pores of the char and in the boundary layer of the particle. The volumetric rate of carbon monoxide consumption is given by Dryer and Glassman (1973):

$$r_{CO} = k_{CO} C_{CO},$$

where

$$k_{CO} = 2.23 \times 10^{12} (C_{H_2O})^{0.5} \left(\frac{C_{O_2}}{2}\right)^{1/4} \exp(-20,130/T),\ \text{s}^{-1}. \tag{3}$$

The formation of NO from char-bound nitrogen (all char-N is oxidized to NO) is assumed proportional to the combustion rate of char (Rajan & Wen, 1980; Song, Beer, & Sarofim, 1982). So, the rate expression of NO formation is:

$$r_{\text{form}} = r_{\text{oxdn}} F_{\text{N,ch}}. \tag{4}$$

The nitrogen oxide formed may be reduced by char according to the reaction (5) in Table 1. As shown by Aarna and Suuberg (1997), there is a considerable difference between the literature rate constants of this reaction. As a first attempt, the average rate expression developed by Aarna and Suuberg (1997) was tested:

$$r_{\text{dest}} = k_{\text{dest}} C_{\text{NO}}, \tag{5}$$

where

$$k_{\text{dest}} = 1.527 \exp(-15,939/T) \frac{RT}{M_{\text{NO}}} a_{\text{ch}},\ \text{s}^{-1}. \tag{5a}$$

2.2.2. Model development

The combustion was described as occurring over the entire volume of the particle. The model is based on: mass transfer and diffusion in the pore system of the char particle, heat transfer and heat conduction in the char particle, heterogeneous reactions of char with oxygen and carbon dioxide, and the evolution of the pore structure and particle diameter. The mass balance equations for oxygen, carbon monoxide, carbon dioxide and nitrogen oxide, following the reaction–diffusion approach, and the heat balance equation are the following:

$$\frac{\partial}{\partial t}(\varepsilon_{p,\text{ch}} y_{\text{O}_2,\text{ch}}) = \frac{\partial}{\partial r}\left(D^{\text{eff}}_{\text{O}_2,\text{ch}} \frac{\partial y_{\text{O}_2,\text{ch}}}{\partial r}\right) + \frac{2D^{\text{eff}}_{\text{O}_2,\text{ch}}}{r} \frac{\partial y_{\text{O}_2,\text{ch}}}{\partial r} - \frac{RT}{P}\left(\frac{\alpha+2\beta}{2(\alpha+\beta)} r_{\text{oxdn}} - \frac{1}{2} r_{\text{form}} F_{\text{N,ch}}\right), \tag{6}$$

$$\frac{\partial}{\partial t}(\varepsilon_{p,\text{ch}} y_{\text{CO,ch}}) = \frac{\partial}{\partial r}\left(D^{\text{eff}}_{\text{CO,ch}} \frac{\partial y_{\text{CO,ch}}}{\partial r}\right) + \frac{2D^{\text{eff}}_{\text{CO,ch}}}{r} \frac{\partial y_{\text{CO,ch}}}{\partial r} + \frac{RT}{P}\left(\frac{\alpha}{\alpha+\beta} r_{\text{oxdn}} + 2r_{\text{gasn}} + r_{\text{dest}}\right), \tag{7}$$

$$\frac{\partial}{\partial t}(\varepsilon_{p,\text{ch}} y_{\text{CO}_2,\text{ch}}) = \frac{\partial}{\partial r}\left(D^{\text{eff}}_{\text{CO}_2,\text{ch}} \frac{\partial y_{\text{CO}_2,\text{ch}}}{\partial r}\right) + \frac{2D^{\text{eff}}_{\text{CO}_2,\text{ch}}}{r} \frac{\partial y_{\text{CO}_2,\text{ch}}}{\partial r} + \frac{RT}{P}\left(\frac{\beta}{\alpha+\beta} r_{\text{oxdn}} - r_{\text{gasn}}\right), \tag{8}$$

$$\frac{\partial}{\partial t}(\varepsilon_{p,\text{ch}} y_{\text{NO,ch}}) = \frac{\partial}{\partial r}\left(D^{\text{eff}}_{\text{NO,ch}} \frac{\partial y_{\text{NO,ch}}}{\partial r}\right) + \frac{2D^{\text{eff}}_{\text{NO,ch}}}{r} \frac{\partial y_{\text{NO,ch}}}{\partial r} + \frac{RT}{P}(r_{\text{form}} - r_{\text{dest}}), \tag{9}$$

$$(\varepsilon_{p,\text{ch}} \rho_G c_{pG} + (1-\varepsilon_{p,\text{ch}}) \rho_{\text{ch}} c_{p,\text{ch}}) \frac{\partial T_{\text{ch}}}{\partial t} = \frac{\partial}{\partial r}\left(\lambda^{\text{eff}}_{\text{ch}} \frac{\partial T_{\text{ch}}}{\partial r}\right) + \frac{2\lambda^{\text{eff}}_{\text{ch}}}{r} \frac{\partial T_{\text{ch}}}{\partial r} + \sum_{i=1}^{4} (-\Delta H_{R,i}) r_i. \tag{10}$$

The relevant boundary conditions are:

$$r = 0, \quad \frac{\partial y_{j,\text{ch}}}{\partial r} = \frac{\partial T_{\text{ch}}}{\partial r} = 0, \tag{11}$$

$$r = r_p(t), \quad D^{\text{eff}}_{j,\text{ch}} \left.\frac{\partial y_{j,\text{ch}}}{\partial r}\right|_{r=r_p} = k_{G,j}(y_{j,\text{ch},s} - y_{j,G}), \tag{12}$$

$$\lambda^{\text{eff}}_{\text{ch}} \left.\frac{\partial T_{\text{ch}}}{\partial r}\right|_{r=r_p} = \alpha_G (T_G - T_{\text{ch},s}). \tag{13}$$

For $\phi^2/Sh < 0.1$, the char particle diameter remains constant and char density, porosity and surface area were calculated as a function of carbon conversion, using the following relationships (Kulasekaran, Linjewile, & Agarwal, 1999; Broden, 1994):

$$\rho_{\text{ch}}/\rho^{\text{in}}_{\text{ch}} = 1 - x_{\text{ch}}, \quad \varepsilon_{p,\text{ch}} = 1.0 - (1.0 - \varepsilon^{\text{in}}_{p,\text{ch}}) \frac{\rho_{\text{ch}}}{\rho^{\text{in}}_{\text{ch}}},$$

$$a_{\text{ch}}/a^{\text{in}}_{\text{ch}} = 1 - x_{\text{ch}}. \tag{14}$$

For $0.1 < \phi^2/Sh < 100$, char particle diameter, density, porosity and surface area were calculated as a function of carbon conversion (Kulasekaran et al., 1999; Broden, 1994):

$$d_p/d^{\text{in}}_p = (1 - x_{\text{ch}})^{1/4}, \quad \rho_{\text{ch}}/\rho^{\text{in}}_{\text{ch}} = (1 - x_{\text{ch}})^{1/4},$$

$$\varepsilon_{p,\text{ch}} = 1.0 - (1.0 - \varepsilon^{\text{in}}_{p,\text{ch}}) \frac{\rho_{\text{ch}}}{\rho^{\text{in}}_{\text{ch}}}, \quad a_{\text{ch}}/a^{\text{in}}_{\text{ch}} = 1 - x_{\text{ch}}. \tag{15}$$

For $\phi^2/Sh > 100$, the density, porosity and internal surface area remain constant. The change in char particle diameter as a function of carbon conversion is

$$d_p/d^{\text{in}}_p = (1 - x_{\text{ch}})^{1/3}. \tag{16}$$

The convective mass and heat transfer coefficients were calculated from the Sherwood and Nusselt numbers:

$$k_{G,j} = \frac{Sh\, D_j}{d_p},$$

where

$$Sh = 2.0\varepsilon + 0.69 \frac{(u_G - u_{\text{ch}}) d_p \rho_G}{\varepsilon \mu_G} Sc^{1/3} \text{ (Basu, 1999)}, \tag{17}$$

$$\alpha_G = \frac{Nu\, \lambda_G}{d_p}, \quad \text{where } Nu = 2.0 + 0.69\, Re_p^{0.5}\, Pr^{1/3}$$

(Field, Gill, Morgan, & Hawksley, 1967). (18)

The effective thermal conductivity of the char was calculated with the following correlation (Kaviany, 1991):

$$\lambda_{\mathrm{ch}}^{\mathrm{eff}} = \lambda_{\mathrm{ch}} \left[1 + \frac{3\varepsilon_{\mathrm{ch}}(1 - (\lambda_{\mathrm{ch}}/\lambda_G))}{(1-\varepsilon_{\mathrm{ch}}) + (\lambda_{\mathrm{ch}}/\lambda_G)(2+\varepsilon_{\mathrm{ch}})} \right]. \tag{19}$$

The effective diffusivity in the char particle was estimated using $D_{j,\mathrm{ch}}^{\mathrm{eff}} = D_j \varepsilon_{p,\mathrm{ch}}^2$. The molecular diffusivities were calculated with the correlations developed by Massman (1998). Finally, the α/β ratio was calculated using $\alpha/\beta = 1860 \exp(-7200/T)$ (Rossberg, 1956; Kulasekaran, Linjewile, Agarwal, & Biggs, 1998).

2.3. Calcination sub-model

Calcination was described as occurring over the entire volume of the particle, with different extents of calcination at different radial locations (Hu & Scaroni, 1996; Khinast, Krammer, Brunner, & Staudinger, 1996). The calcination model is based on: mass transfer and diffusion in the pore system of the particle, heat transfer and heat conduction in the particle, surface decomposition of $CaCO_3$ when a non-equilibrium condition exists, and the evolution of the pore structure. The effect of sintering was omitted and the size and shape of the spherical particle is assumed to remain unchanged throughout the course of the calcination. The variation of the heat of reaction with the temperature is neglected.

Thermal decomposition. As a solid–gas decomposition reaction, the calcination of limestone occurs at a solid $CaCO_3$ surface when the local conditions exceed the equilibrium decomposition criterion established from the work of Baker (1962) and Hu and Scaroni (1996) as

$$P_{\mathrm{CO}_2,e} = 1.886 \times 10^{12} \exp(-19,680/T), \ \mathrm{Pa}. \tag{20}$$

The reaction rate at the external and internal surface is expressed as (Hu & Scaroni, 1996):

$$r_c = k_c \frac{P_{\mathrm{CO}_2,e} - P_{\mathrm{CO}_2}}{P_{\mathrm{CO}_2,e}}, \quad 10^{-2} P_{\mathrm{CO}_2,e} < P_{\mathrm{CO}_2} < P_{\mathrm{CO}_2,e}, \tag{21}$$

$$r_c = k_c, \quad P_{\mathrm{CO}_2} < 10^{-2} P_{\mathrm{CO}_2,e}. \tag{22}$$

The reaction rate constant given by Borgwardt (1985) was modified. This constant was related to the reaction surface area according to the modified random pore model (Khinast et al., 1996):

$$k_c = 247.8 \exp(-24,660/T), \ \mathrm{kmol/m^2 s}. \tag{23}$$

From the solid reactant balance, the calcination rate can be expressed in terms of conversion as (Khinast et al., 1996)

$$\frac{\partial x_c}{\partial t} = r_c S_v M_{\mathrm{CaCO_3}}, \tag{24}$$

where the local specific reaction surface area S_v is related to the solid conversion as (Khinast et al., 1996)

$$\frac{S_v}{S_v^{\mathrm{in}}} = (1-x_c)[1 - \Psi \ln(1-x_c)]^{1/2}. \tag{25}$$

The relationship between overall conversion and local conversion is given by

$$\overline{x_c(t)} = \frac{3}{R_p^3} \int_0^{R_p} r^2 x_c(r,t)\, \mathrm{d}r. \tag{26}$$

Particle-scale model. The unsteady-state CO_2 diffusion equation is

$$\frac{\partial}{\partial t}(\varepsilon_{p,c} y_{\mathrm{CO}_2,c}) = \frac{\partial}{\partial r}\left(D_{\mathrm{CO}_2,c}^{\mathrm{eff}} \frac{\partial y_{\mathrm{CO}_2,c}}{\partial r} \right) + \frac{2 D_{\mathrm{CO}_2,c}^{\mathrm{eff}}}{r} \frac{\partial y_{\mathrm{CO}_2,c}}{\partial r} + r_c S_v \rho_c \frac{R T_c}{P} \tag{27}$$

with the boundary conditions

$$r = 0, \quad \frac{\partial y_{\mathrm{CO}_2,c}}{\partial r} = 0, \tag{28}$$

$$r = R_p, \quad D_{\mathrm{CO}_2,c}^{\mathrm{eff}} \left. \frac{\partial y_{\mathrm{CO}_2,c}}{\partial r} \right|_{r=R_p} = k_G (y_{\mathrm{CO}_2,G} - y_{\mathrm{CO}_2,c,s}). \tag{29}$$

The particle porosity was calculated as a function of the conversion, final and initial porosity (Khinast et al., 1996):

$$\frac{\varepsilon_{p,c}}{\varepsilon_{p,c}^{\mathrm{in}}} = 1 + x_c \left(\frac{\varepsilon_{p,c}^{\mathrm{e}}}{\varepsilon_{p,c}^{\mathrm{in}}} - 1 \right). \tag{30}$$

For a spherical particle, the unsteady-state heat transfer equation is

$$[\varepsilon_{p,c}\rho_G c_{pG} + (C_{\mathrm{CaCO_3}} c_{p,\mathrm{CaCO_3}} + C_{\mathrm{CaO}} c_{p,\mathrm{CaO}})(1-\varepsilon_{p,c})] \times \frac{\partial T_c}{\partial t} = \frac{\partial}{\partial r}\left(\lambda_c^{\mathrm{eff}} \frac{\partial T_c}{\partial r} \right) + \frac{2\lambda_c^{\mathrm{eff}}}{r} \frac{\partial T_c}{\partial r} + (-\Delta H_c) r_c S_v \rho_c, \tag{31}$$

$$r = 0, \quad \frac{\partial T_c}{\partial r} = 0, \tag{32}$$

$$r = R_p, \quad \lambda_c^{\mathrm{eff}} \left. \frac{\partial T_c}{\partial r} \right|_{r=R_p} = \alpha_G (T_G - T_{c,s}). \tag{33}$$

For limestone calcination, the thermal conductivity depends on the state of the solid material. The value of thermal conductivity differs greatly among uncalcined, partially calcined and fully calcined material. For partially calcinated material, the conductivity was calculated with the following relationship (Hu & Scaroni, 1996).

$$\lambda_c^{\mathrm{eff}} = \frac{1}{[(1-x_c)/\lambda_{\mathrm{CaCO_3}}] + (x_c/\lambda_{\mathrm{CaO}})}. \tag{34}$$

Sherwood and Nusselt numbers were calculated using the empirical correlations developed by Basu (1999) and Field et al. (1967).

The effective diffusion of the carbon dioxide includes both Knudsen and molecular diffusion (Keener & Khang, 1992). The molecular diffusivity of the carbon dioxide was calculated with the correlation developed by Massman (1998). The evaluation of Knudsen diffusivity through the CaO layer was carried out by the equation (Saterfield, 1970)

$$D_K = 97 r_{\text{pore}} \sqrt{\frac{T}{M_{CO_2}}}, \tag{35}$$

where $r_{\text{pore}} = 0.1 \times 10^{-6}$ m (Keener & Khang, 1992).

2.4. Reactor-scale model

2.4.1. Reaction network

Three groups of chemical reactions are included in the reactor-scale model (Table 2): homogeneous and heterogeneous gas–solid and catalyzed reactions. In the case of catalytic reactions, the effectiveness factor is assumed equal to 1 due to the small diameter of the char particles. NH_3 was considered as an intermediate component in HCN oxidation: $HCN + H_2O \rightarrow NH_3 + CO$ (Mitchell & Tarbell, 1982).

2.4.2. Model development

The model for the gas phase is comprised of unsteady-state mass balance equations written for each of the chemical species considered in the calciner. This model is coupled with the char combustion and calcination model by the mass and heat fluxes at the particle surfaces. The reducing and oxidizing zones were assumed operated under adiabatic conditions. As shown by Wei et al. (1993), Wei and Zhu (1996) and Namkung and Kim (1998), gas backmixing is very important in dilute zone of fluidized beds and in fast fluidization regime, especially in the industrial units. So, because calciners are dilute systems operating in the pneumatic transport regime, an axial dispersion model was adopted for the gas and solid phases. The model equations for the reducing zone are the following:

$$\varepsilon_G \frac{\partial y_{O_2,G}}{\partial t} + u_G \frac{\partial y_{O_2,G}}{\partial z} = D_G \varepsilon_G \frac{\partial^2 y_{O_2,G}}{\partial z^2} - D^{\text{eff}}_{O_2,\text{ch}} \times \left.\frac{\partial y_{O_2,\text{ch}}}{\partial r}\right|_{r=r_p} a_s + \frac{RT_G}{P} \sum_{i=1}^{n} \nu_{i,O_2} r_i, \tag{36}$$

$$\varepsilon_G \frac{\partial y_{CO,G}}{\partial t} + u_G \frac{\partial y_{CO,G}}{\partial z} = D_G \varepsilon_G \frac{\partial^2 y_{CO,G}}{\partial z^2} - D^{\text{eff}}_{CO,\text{ch}} \times \left.\frac{\partial y_{CO,\text{ch}}}{\partial r}\right|_{r=r_p} a_s + \frac{RT_G}{P} \sum_{i=1}^{n} \nu_{i,CO} r_i, \tag{37}$$

$$\varepsilon_G \frac{\partial y_{CO_2,G}}{\partial t} + u_G \frac{\partial y_{CO_2,G}}{\partial z} = D_G \varepsilon_G \frac{\partial^2 y_{CO_2,G}}{\partial z^2} - D^{\text{eff}}_{CO_2,\text{ch}} \left.\frac{\partial y_{CO_2,\text{ch}}}{\partial r}\right|_{r=r_p} a_s - D^{\text{eff}}_{CO_2,c} \left.\frac{\partial y_{CO_2,c}}{\partial r}\right|_{r=R_p} a'_s + \frac{RT_G}{P} \sum_{i=1}^{n} \nu_{i,CO_2} r_i \tag{38}$$

$$\varepsilon_G \frac{\partial y_{NO,G}}{\partial t} + u_G \frac{\partial y_{NO,G}}{\partial z} = D_G \varepsilon_G \frac{\partial^2 y_{NO,G}}{\partial z^2} - D^{\text{eff}}_{NO,\text{ch}} \left.\frac{\partial y_{NO,\text{ch}}}{\partial r}\right|_{r=r_p} a_s + \frac{RT_G}{P} \sum_{i=1}^{n} \nu_{i,NO} r_i, \tag{39}$$

$$\varepsilon_G \frac{\partial y_{j,G}}{\partial t} + u_G \frac{\partial y_{j,G}}{\partial z} = D_G \varepsilon_G \frac{\partial^2 y_{j,G}}{\partial z^2} + \frac{RT_G}{P} \sum_{i=1}^{n} \nu_{i,j} r_i, \tag{40}$$

where $j = H_2, NH_3, H_2O, C_3H_8, C_2H_4, C_{18}H_{12}, CH_4$.

$$\varepsilon_G \rho_G c_{pG} \frac{\partial T_G}{\partial t} + u_G \rho_G c_{pG} \frac{\partial T_G}{\partial z} = \varepsilon_G \lambda_G \frac{\partial^2 T_G}{\partial z^2} - \lambda^{\text{eff}}_{\text{ch}} \left.\frac{\partial T_{\text{ch}}}{\partial r}\right|_{r=r_p} a_s - \lambda^{\text{eff}}_{c} \left.\frac{\partial T_c}{\partial r}\right|_{r=R_p} a'_s + \sum_{i=1}^{n} (-\Delta H_{Ri}) r_i \tag{41}$$

$$z = 0, \quad u_G y_{j,G}|_{z=0^-} = u_G y_{j,G}|_{z=0^+} - \varepsilon_G D_G \frac{\partial y_{j,G}}{\partial z}, \tag{42}$$

$$\rho_G c_{pG} u_G T_G|_{z=0^-} = \rho_G c_{pG} u_G T_G|_{z=0^+} - \lambda_G \frac{\partial T_G}{\partial z}, \tag{43}$$

$$z = H, \quad \frac{\partial y_{j,G}}{\partial z} = \frac{\partial T_G}{\partial z} = 0. \tag{44}$$

In the oxidizing zone, the mass balance equation for oxygen was modified to take into account the gradual mixing of preheated combustion air into the main flow. A modified Zwietering approach, in which the degree of mixing as a function of calciner residence time is given by Jensen (1999) [degree of mixing $= 1 - \exp(-k_{\text{mix}}\, \bar{t} z/H)$], was employed for O_2, whereas the N_2 in the preheated combustion air was assumed to mix instantaneously into the kiln flue gas. The mass balance equation for oxygen is thus:

$$\varepsilon_G \frac{\partial y_{O_2,G}}{\partial t} + u_G \frac{\partial y_{O_2,G}}{\partial z} + y_{O_2,G} \frac{\partial u_G}{\partial z} = D_G \varepsilon_G \frac{\partial^2 y_{O_2,G}}{\partial z^2} - D^{\text{eff}}_{O_2,\text{ch}} \left.\frac{\partial^2 y_{O_2,\text{ch}}}{\partial r}\right|_{r=r_p} a_s + \frac{RT_G}{P} \sum_{i=1}^{n} \nu_{i,O_2} r_i + k_{\text{mix}}\, y^{\text{in}}_{O_2,G} \exp\left(-k_{\text{mix}}\, \bar{t}\, \frac{z}{H}\right), \tag{45}$$

where

$$\frac{du_G}{dz} = \frac{D^{\text{oxdn}}_{VG}}{SH} k_{\text{mix}} y^{\text{in}}_{O_2} \bar{t} \exp\left(-k_{\text{mix}}\, \bar{t}\, \frac{z}{H}\right). \tag{46}$$

Table 2
Heterogeneous and homogeneous reactions included in the reactor-scale model

Reaction	Catalyst	Rate constant	Reference
$NH_3 + NO + \frac{1}{4}O_2 \rightarrow N_2 + \frac{3}{2}H_2O$	Homog.	$k_1 = 2.45 \times 10^{14} \exp\left(\frac{-29,400}{T}\right)$,	Duo, Dam-Johansen, and Ostergaard (1992)
$r_1 = k_1 C_{NH_3} C_{NO}$		$m^3/mol\ s$	
$NH_3 + \frac{5}{4}O_2 \rightarrow NO + \frac{3}{2}H_2O$	Homog.	$k_2 = 2.21 \times 10^{14} \exp\left(\frac{-38,160}{T}\right)$	Duo et al. (1992)
$r_2 = k_2 C_{NH_3}$		s^{-1}	
$H_2 + \frac{1}{2}O_2 \rightarrow H_2O$	Homog.	$k_3 = 1.631 \times 10^6 T^{3/2} \exp\left(\frac{-3420}{T}\right)$	Vilienskii and Hezmalian (1978)
$r_3 = k_3 C_{H_2}^{3/2} C_{O_2}$		$m^3/kmol\ s$	
$NO + H_2 \rightarrow H_2O + \frac{1}{2}N_2$	Char	$k_4 = 4.6T \exp\left(\frac{-12,120}{T}\right)$	Furusawa, Tsunoda, and Kunii, (1982).
$r_4 = k_4 C_{NO} C_{H_2}$	CaO	$k_4' = 7 \times 10^{10} \exp\left(\frac{-9320}{T}\right)$	Tsujimura, Furusawa, and Kunii (1983a)
		$m^3/kmol\ s$	
$NO + CO \rightarrow CO_2 + \frac{1}{2}N_2$		$k_1 = 2.1 \times 10^{-6} \exp\left(\frac{-13,100}{T}\right)$	Chan, Sarofim, and Beer (1983)
$r_5 = \frac{k_1 P_{NO}(k_2 P_{CO} + k_3)}{k_1 P_{NO} + k_2 P_{CO} + k_3}$	Char	$kmol/m^2\ s\ Pa$	
		$k_2 = 7.3 \times 10^{-9} \exp\left(\frac{-9560}{T}\right)$	
		$kmol/m^2\ s\ Pa$	
		$k_3 = 0.015 \exp\left(\frac{-20,100}{T}\right)$	
		$kmol/m^2\ s$	
$r_5' = k_5' C_{NO} C_{CO}$	CaO	$k_5' = 1.58 \times 10^8 \exp\left(\frac{-8920}{T}\right)$	Tsujimura, Furusawa, and Kunii (1983b)
		$ppm^{-1}\ s^{-1}$	
$NH_3 + \frac{5}{4}O_2 \rightarrow NO + \frac{3}{2}H_2O$			Furusawa, Tsujimura, Yasunaga, and Kojima (1985)
$r_6 = k_6 C_{NH_3} C_{O_2}$	Char	$k_6 = 4.95 \times 10^{12} \exp\left(\frac{-15,000}{T}\right)$	
		$m^3/kmol\ s$	
$r_6' = k_6' C_{NH_3} C_{O_2}$	CaO	$k_6' = 2.67 \times 10^{10} \exp\left(\frac{-10,000}{T}\right)$	Furusawa et al. (1985)
		$m^3/kmol\ s$	
		($E/R = 15,000$, and 10,000 respectively, were used for temperature correction)	
$NH_3 + NO + \frac{1}{4}O_2 \rightarrow N_2 + \frac{3}{2}H_2O$	CaO	$k_7 = 0.73 \times 10^6 \exp\left(\frac{-7000}{T}\right) s^{-1}$	Chambers, Yoshii, Inada, and Miyamoto (1996)
$r_7 = k_7 C_{NH_3}$			
$C_3H_8 \rightarrow \frac{3}{2}C_2H_4 + H_2$	Homog.	$k_8 = 2.57 \times 10^{13} \exp\left(\frac{-24,962}{T}\right)$	Hautman, Dryer, Schug, and Glassman (1981)
$r_8 = k_8 C_{C_3H_8}^{0.5} C_{O_2}^{1.07} C_{C_2H_4}^{0.4}$ $(kmol/m^3\ s)$			
$C_2H_4 + O_2 \rightarrow 2CO + 2H_2$	Homog.	$k_9 = 3.71 \times 10^{12} \exp\left(\frac{-25,163}{T}\right)$	Hautman et al. (1981)
$r_9 = k_9 C_{C_2H_4}^{0.9} C_{O_2}^{1.18} C_{C_3H_8}^{-0.37}$ $(kmol/m^3\ s)$			
$C_{18}H_{12} + 21O_2 \rightarrow 6H_2O + 18CO_2$	Homog.	$k_{10} = 1.8 \times 10^{10} \exp\left(\frac{-15,844.77}{T}\right)$	Dernedde, Charette, Bourgeois, and Castonguay (1986)
$r_{10} = k_{10} C_{C_{18}H_{12}} C_{O_2}^{1/2} C_{H_2O}^{1/2}$ $(kmol/m^3\ s)$			
$CH_4 + 2O_2 \rightarrow 2H_2O + CO_2$	Homog.	$k_{11} = 2.99 \times 10^{10} \exp\left(\frac{-23,634.2}{T}\right)$	Bradley, Chin, and Draper (1976)
$r_{11} = k_{11} C_{CH_4}^{0.7} C_{O_2}^{0.8}$ $(kmol/m^3\ s)$			
$2NH_3 + \frac{3}{2}O_2 \rightarrow N_2 + 3H_2O$			Furusawa et al. (1985)
$r_{12} = k_{12} C_{NH_3} C_{O_2}$	Char	$k_{12} = 1.58 \times 10^{13} \exp\left(\frac{-15,000}{T}\right)$	
		$m^3/kmol\ s$	
$r_{12}' = k_{12}' C_{NH_3} C_{O_2}$	CaO	$k_{12} = 6.65 \times 10^9 \exp\left(\frac{-10,000}{T}\right)$	
		$m^3/kmol\ s$	
		($E/R = 15,000$, and 10,000 respectively were used for temperature correction)	

Also, all mass balance equations were modified to take into account the variation of the gas velocity in the reactor.

The carbon concentration in the calciner is dictated by the burning rate of individual char particle. Both mass transfer of oxygen and the chemical reaction rate of combustion govern this rate. The mass balance equation for the carbon is as follows:

$$\frac{\partial C_{\mathrm{ch}}}{\partial t} + v_{\mathrm{ch}}\frac{\partial C_{\mathrm{ch}}}{\partial z} = D_s\frac{\partial^2 C_{\mathrm{ch}}}{\partial z^2} - qM_{\mathrm{ch}} \tag{47}$$

with the boundary conditions:

$$z = 0, \quad v_{\mathrm{ch}}C_{ch}|_{z=0^-} = v_{\mathrm{ch}}C_{\mathrm{ch}}|_{z=0^+} - D_s\frac{\partial C_{\mathrm{ch}}}{\partial z}, \tag{48}$$

$$z = H, \quad \frac{\partial C_{\mathrm{ch}}}{\partial z} = 0, \tag{49}$$

where the burning rate (q) is given as (Basu & Fraser, 1991, Chap. 4; Basu, 1999)

$$q = \frac{k_1 k_2 P_{\mathrm{O}_2,G}}{k_2 + k_1' + k_1 P_{\mathrm{O}_2,G}}\eta. \tag{50}$$

The inlet char concentration ($C_{\mathrm{ch}}|_{z=0^-}$) was calculated using the model developed by Timar and Mierka (1997).

Finally, the mass balance equation for the limestone in the calciner is as follows (with the boundary conditions (46), (47)):

$$\frac{\partial C_c}{\partial t} + v_c\frac{\partial C_c}{\partial z} = D_s\frac{\partial^2 C_c}{\partial z^2} - r_c S_v \rho_{\mathrm{CaCO_3}}. \tag{51}$$

2.5. Gas holdup sub-model

The gas holdup was calculated using the one-dimensional model developed by Nieuwland et al. (1997). This model neglects the existence of clustering particles and lateral solids segregation, which has been found in calciners by Hundebøl and Kumar (1987). It is based on the continuity equations in the gas and solid phases and the momentum equations in axial direction. The final form of the model is represented by the following equations:

$$-\frac{\mathrm{d}P}{\mathrm{d}z} = -[\rho_s(1-\varepsilon_G) + \rho_G\varepsilon_G]g - F_G - F_p + \gamma\frac{\mathrm{d}\varepsilon_G}{\mathrm{d}z}, \tag{52}$$

$$\frac{\mathrm{d}\varepsilon_G}{\mathrm{d}z} = \frac{\beta(v_G - v_s) + \varepsilon_G[(\rho_s - \rho_G)g(1-\varepsilon_G) + F_p] - F_G(1-\varepsilon_G)}{\gamma\varepsilon_G + \rho_G v_G^2}, \tag{53}$$

where

$$\gamma = \rho_s(v_s)^2 - \rho_G v_G^2, \tag{54}$$

$$F_G = -\frac{4f_G\varepsilon_G\rho_G v_G^2}{2d_c}, \quad f_G = \frac{0.0791}{Re^{0.25}}, \quad Re = \frac{\mathrm{d}_c\rho_G u_G}{\mu_G}$$

(Bird, Stewart, & Lightfoot, 1960), (55)

$$F_p = -\frac{4f_p(1-\varepsilon_G)\rho_s(v_s)^2}{2d_c}, \quad 4f_p = \frac{7\times 10^{-5}\rho_s(v_s)^{0.6}}{G_s}$$

(Nieuwland et al., 1997), (56)

$$\beta = \tfrac{3}{4}C_{d,s}\frac{\varepsilon_G(1-\varepsilon_G)}{d_p}\rho_G|v_G - v_s|\varepsilon_G^{-2.65}$$

(Nieuwland et al., 1997), (57)

$$C_{D,s} = \frac{24}{Re_p} + \frac{3.6}{Re_p^{0.313}} \quad \text{(Nieuwland et al., 1997).} \tag{58}$$

The main model assumptions are that the constituted relations for gas–particle interphase drag coefficient, gas–wall friction coefficient and particle–wall friction coefficient remain the same regardless of the acceleration of the gas and particle phases.

2.6. Numerical solution of the model equations

The partial differential equations are coupled non-linear equations involving time and space dependencies for each species and temperature at the particle and the reactor scales simultaneously, and are subject to non-homogeneous boundary conditions. Solutions of the above models require a priori knowledge of several hydrodynamic parameters, mass and heat transfer coefficients, and reaction rate expressions. A computer program was developed in Fortran to solve for each zone of the calciner the corresponding system of two-dimensional parabolic partial differential equations. Normalization of the model was made using the initial concentration in the gas and solid phases and the discretization in the spatial dimension was carried out by the method of orthogonal collocation (Finlayson, 1972; Villadsen & Michelsen, 1978). The number of collocation points specified for the solid particles and reactor are respectively, 3 and 9. The GEAR integration method for stiff differential equations was employed to integrate the resulting time derivatives. The steady-state solution was obtained by integrating the problem through time until the field variables cease to change.

As a function of the trends of the concentration and temperature profiles the mathematical model can be simplified.

3. Results and discussion

The application of the heterogeneous model is illustrated through calculations relevant for both the reducing and the oxidizing zone of an in-line low-NO_x calciner with particular emphasis on the influence of the oxygen mixing into the main flow on the species concentration profiles. Two types of approaches were compared: instantaneous mixing of oxygen into the main flow (i) and gradual mixing of oxygen

Table 3
Analysis of Colorado bituminous coal (wt% as received)

Moisture	2.29
Volatile matter	39.98
Fixed carbon	48.47
Ash	11.55
Carbon	72.12
Hydrogen	5.58
Oxygen	9.17
Nitrogen	1.26
Sulfur	0.59

Table 4
Chemical composition and initial structural properties of raw meal

Composition (*wt*%)	
$CaCO_3$	75.0
SiO_2	15.0
Al_2O_3	2.5
Fe_2O_3	2.5
Other	5.0
Initial structural properties	
BET surface area, m^2/g	1.54
Initial porosity	0.032
True density, kg/m^3	2710

Table 5
Parameters used in simulations

Reducing zone	
Gas velocity: 11 m/s	Reactor diameter 2.5 m
Pressure: 1 atm	Reducing zone height 2.2 m
Inlet temperature: 1223 K	Char particle diameter 50 μm
Inlet molar fraction:	Limestone particle diameter 50 μm
O_2 0.031	Sphericity factor 0.8
CO 0.001	$a_{ch}^{in} = 1.6 \times 10^7\ m^2/m^3$
CO_2 0.19	(Aarna & Suuberg, 1997)
NO 0.000928	$\varepsilon_{ch}^{in} = 0.6$ (Sahu, Levendis, Flagan, & Gavalast, 1988)
Coal mass flow rate: 2.1 kg/s	
Raw meal flow rate: 13.4 kg/s	
$Pe_G = Pe_h = 40, Pe_s = 10$	
Oxidizing zone	
Gas velocity: 5.4 m/s	Reactor diameter 5.75 m
Pressure: 1 atm	Oxidizing zone height 21.0 m
Coal mass flow rate: 2.1 kg/s	Char particle diameter 50 μm
Raw meal flow rate: 31.4 kg/s	Limestone particle diameter 50 μm
$D_{v_G}^{oxdn} = 85\ m^3/s$	
$Pe_G = Pe_h = 40, Pe_s = 10$	

into the main flow at different rates (ii). The validity of the proposed model is tested by employing the model to simulate in-line-calciner operation under the conditions at which full-scale plant measurements were performed by Thomsen et al. (1998), and comparing the model simulated results to the measured data (Thomsen et al., 1998; Jensen, 1999). The operating conditions of the considered in-line-calciner were approximated by the conditions presented in Tables 3–5. As simplifying approximations, the particle size distributions of both the char and limestone were assumed monodisperse

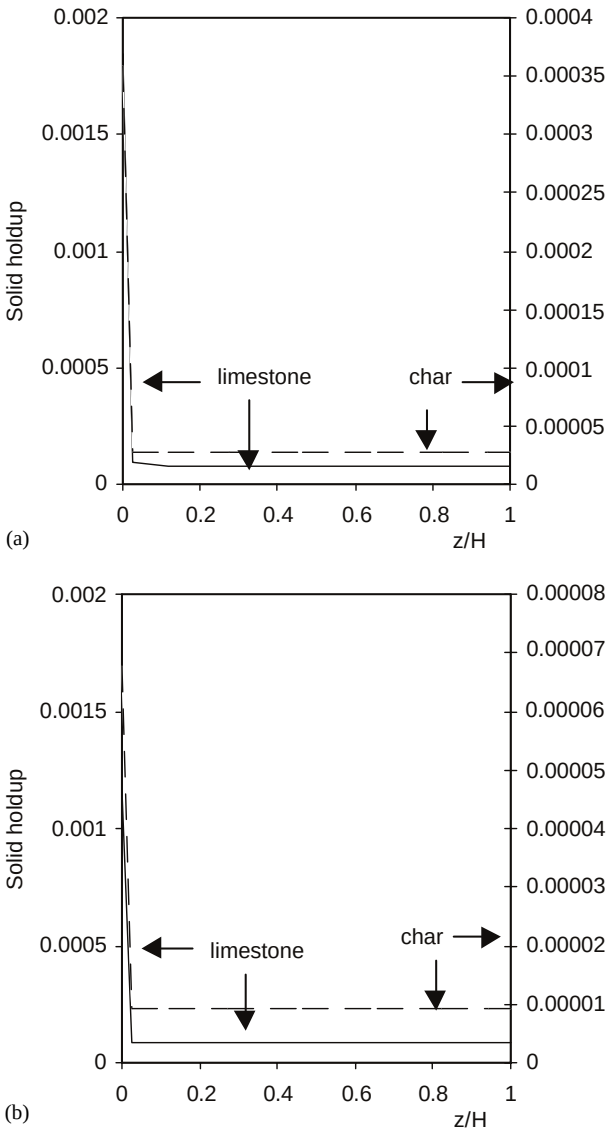

Fig. 2. Solid holdup profiles in the calciner: (a) reducing zone, (b) oxidizing zone.

with diameters of 50 μm. The char properties were based on literature data (Aarna & Suuberg, 1997) and not on analyses of sampled chars.

Fig. 2 presents the model calculated solid holdup profiles in the calciner, Figs. 3 and 4 give typical steady-state concentration and temperature profiles in char and limestone particles at given positions in the calciner and Figs. 5–12 show calculated axial calciner profiles of gaseous species concentrations, degrees of limestone calcination, degrees of carbon conversion and of temperature.

The calculated solid holdup profiles in Fig. 2 indicate that both zones of the calciner are dilute systems in the pneumatic transport regime (solid holdup $\ll 0.01\ m^3/m^3$).

Figs. 3a and 4a show that internal diffusion is important in the reducing zone—both within the char particles and in the limestone particles. In the first part of the oxidizing

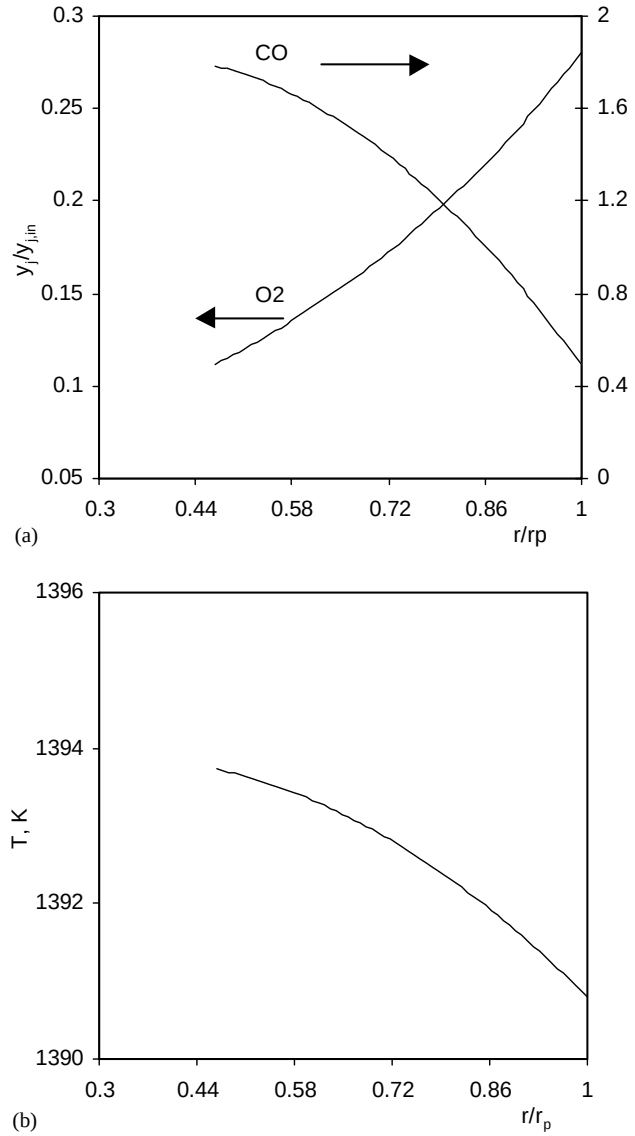

Fig. 3. Concentration and temperature profiles in char particle—reducing zone, $z/H = 0.0237$ ($y_{O_2,in} = 0.0354$, $y_{CO,in} = 7.89 \times 10^{-3}$).

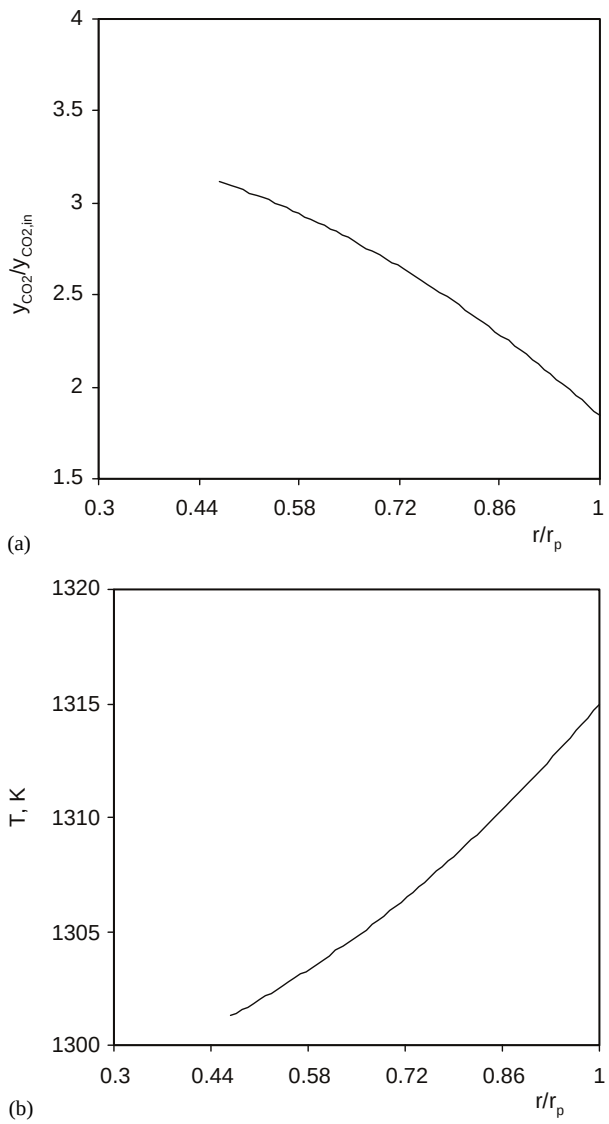

Fig. 4. CO_2 concentration and temperature profiles in limestone particle—reducing zone, $z/H = 0.12$ ($y_{CO_2,in} = 0.1837$).

zone, internal diffusion is also important, though not shown in the figures. In the reducing zone, the difference between the temperature at the char particle periphery and center is approximately 3 K indicating a negligible resistance to internal heat transfer, which means that the char particle may be considered isothermal (as was found to be the case in the oxidizing zone). In the case of limestone particles, the internal heat transfer resistance is important. This is evident in the reducing zone from Fig. 4b, which shows a temperature difference greater than 15 K (the maximum difference is 80 K). The temperature at the periphery of the limestone and char particles is only slightly lower/higher than in the bulk gas, indicating a negligible resistance to external heat transfer. Also, the external mass transfer is not very important.

The oxygen concentration profiles (Fig. 5) through the calciner show that the oxygen concentration in the reducing zone decreases sharply due to the rapid consumption by volatiles combustion, while the behavior in the oxidizing zone depends on the mixing rate. When the preheated combustion air is mixed instantaneously with the sub-stoichiometric suspension leaving the reducing zone, the O_2 concentration drops continuously up through the oxidizing zone. With a slow and intermediate rate of mixing preheated combustion air into the flow (0.7 and 1.4 s^{-1}), the oxygen concentration passes through a maximum at $z/H \approx 0.5$ and 0.3, respectively.

The degree of char conversion in the reducing zone is only 2.0% due to the fact that the oxygen is consumed rapidly by the volatiles combustion reactions, after which it increases up through the oxidizing zone (Fig. 6). After the oxidizing zone, the degree of burnout is highest in the case of instantaneous mixing (99% conversion), and lowest in the case

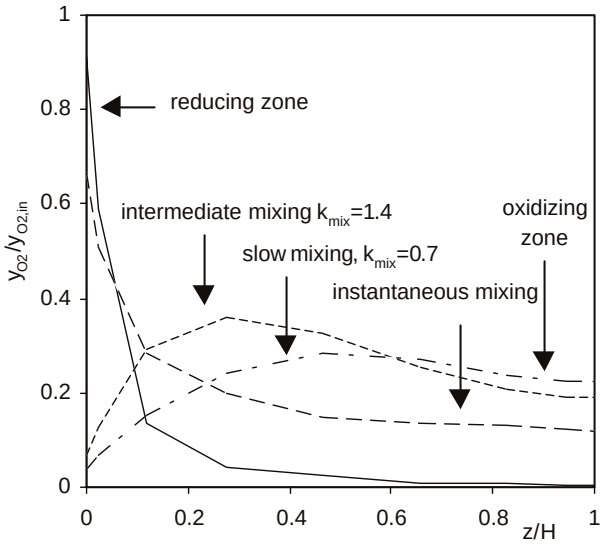

Fig. 5. Variation of the oxygen concentration with the axial distance ($y_{O_2,in} = 0.14$—oxidizing zone, $y_{O_2,in} = 0.0354$—reducing zone).

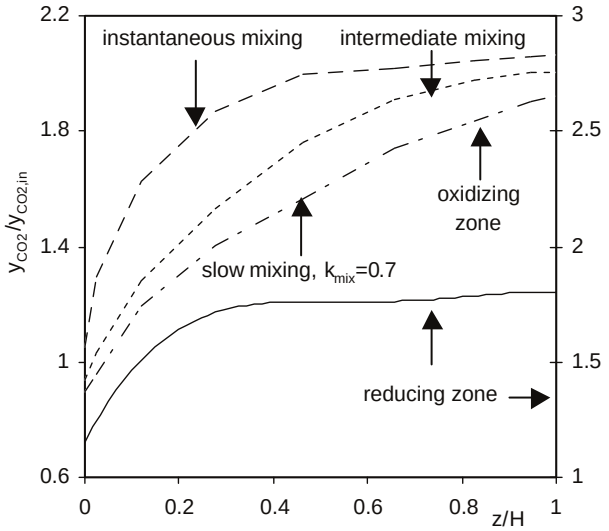

Fig. 7. Variation of CO_2 concentration with the axial distance ($y_{CO_2,in} = 0.1837$).

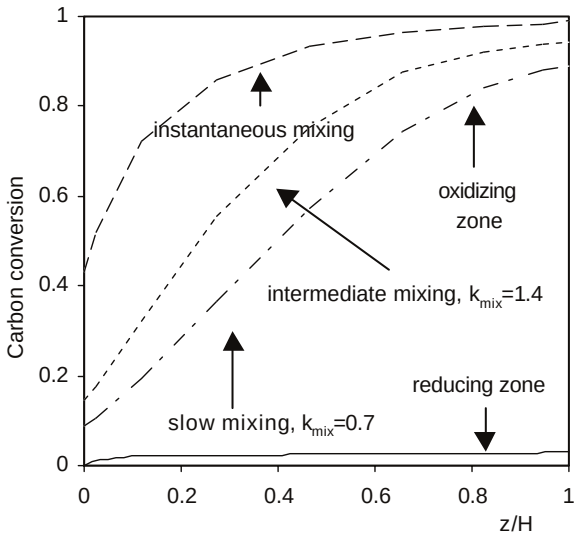

Fig. 6. Variation of carbon conversion with the axial distance.

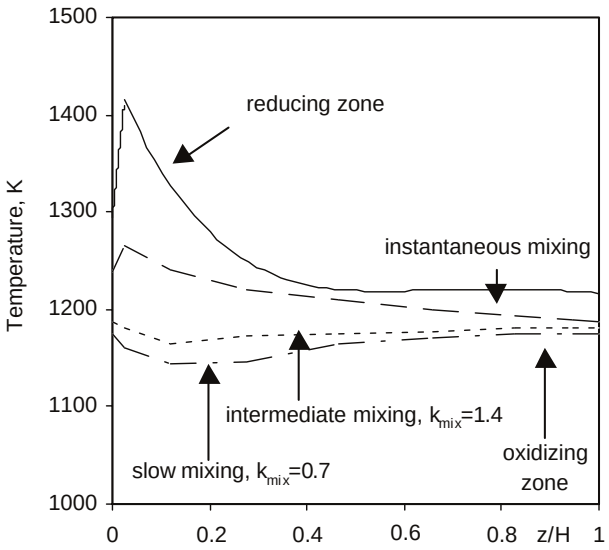

Fig. 8. Variation of the temperature with the axial distance.

of slow mixing (90%). The profile predicted by the model qualitatively corresponds to the trends measured on the considered full-scale calciner (Thomsen et al., 1998; Jensen, 1999). The mixing rate was found only to have a significant effect on char burnout at low values of mixing rate constant ($< 20\ s^{-1}$). When the mixing of oxygen is slow, carbon conversion (Fig. 6) increases slowly in the first part of the calciner due to the low concentration of oxygen, which results in a low rate of char combustion.

As a consequence of the low local O_2 concentration in the case of slow mixing of preheated combustion air into the bulk flow, the CO_2 concentration increases slowly (Fig. 7) due to the low rate of heat release from the burning fuel, resulting in slow CO_2 formation both from combustion and calcination. The effect is reinforced by the lower rate of heat release also resulting in a lower calciner temperature, which further reduces the combustion rate and thereby also the rate of heat release (Fig. 8). The temperature in the bottom of the oxidizing zone is observed to be 100 K higher when preheated combustion air is instantaneously mixed into the flow than when slowly mixed (Fig. 8). In the second part of the oxidizing zone, the temperature is not significantly affected by the mixing rate. At the bottom of the reducing zone (Fig. 8), the temperature increases very steeply due to the combustion of volatiles. Subsequently, insignificant heat generation by combustion due to oxygen deficiency accompanied by strong heat consumption by calcination results in the temperature decrease in the second part of reducing zone.

The extent of calcination follows the evolution of CO_2 concentration (Fig. 9), and is affected by mixing as explained

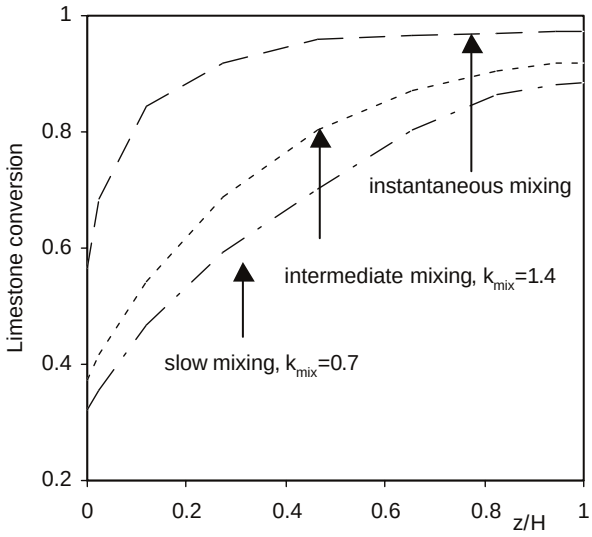

Fig. 9. Variation of the limestone conversion with the axial distance (oxidizing zone).

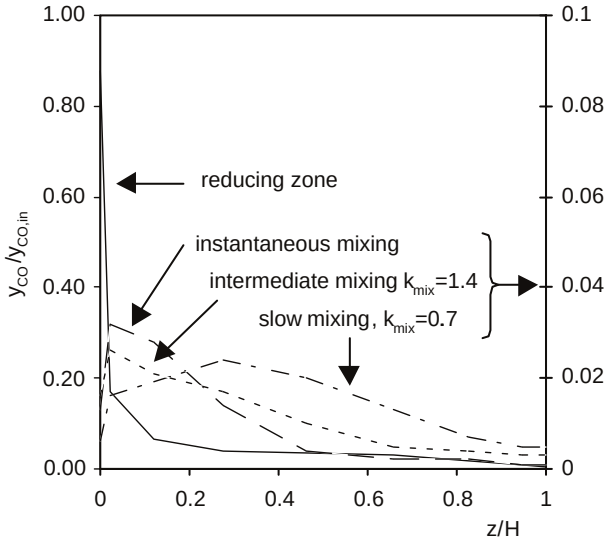

Fig. 11. Variation of CO concentration with the axial distance ($y_{CO,in} = 7.89 \times 10^{-3}$).

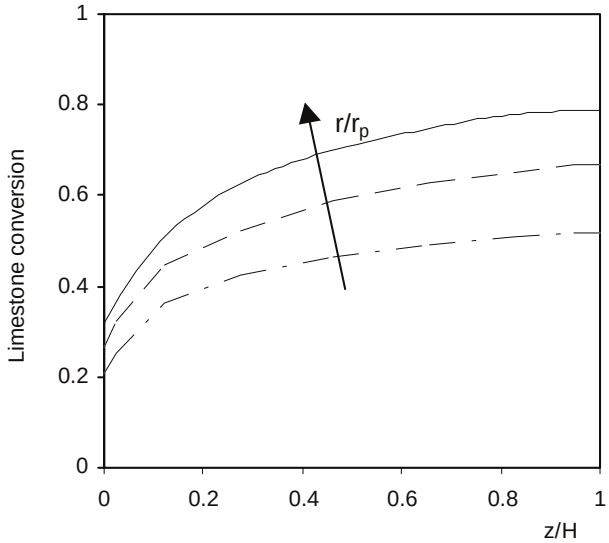

Fig. 10. Extent of calcination as a function of axial reactor distance and radial position of the particle (reducing zone).

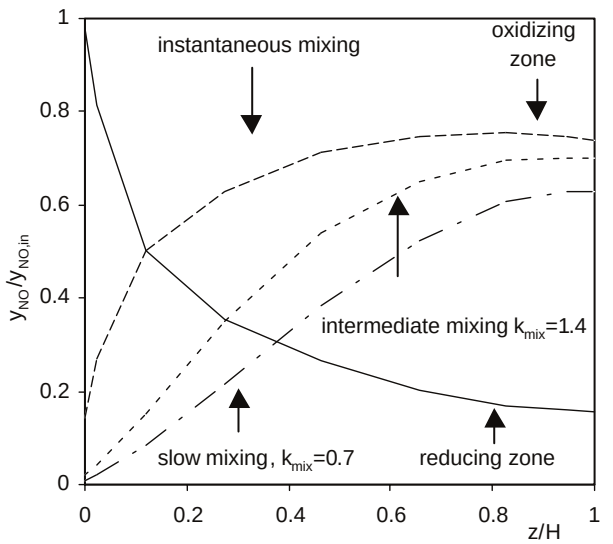

Fig. 12. Variation of NO concentration with the axial distance ($y_{NO,in} = 8.9 \times 10^{-4}$).

above. With a mixing rate (k_{mix}) of 1.4 s^{-1}, the calculated degree of limestone calcination at the calciner exit corresponds approximately to measured full-scale data (Jensen, 1999). Therefore, the limestone calcination conversion in the calciner of this plant suggests an intermediate value for oxygen mixing rate.

Fig. 10 shows the profiles of the limestone conversion (for the reducing zone) at the reactor level and different radial position of the particle. In accordance with the earlier conclusions that both resistances to internal heat and mass transfer within limestone particles are important to take into account, the model predicts a small difference in the extent of calcination between the particle periphery and the particle center at the beginning of reducing zone, the difference increasing in the second part. Thus the calcination of dispersed limestone particles is not under chemical kinetic control in the reducing zone.

Fig. 11 shows CO concentration profiles for the two zones of the calciner. In the reduction zone, the CO concentration decreases rapidly, while a local maximum is observed in the oxidizing zone at all mixing rates. In the case of rapid mixing, the initial CO peak is higher and drops more rapidly than in the case of slow mixing. The exit CO concentration is higher in the case of slow mixing.

In the presence of CO, NO may be catalytically reduced in the local absence of oxygen (Van den Bleek & Van den

Berg, 1980). Due to the inhibiting effect of oxygen, the raw meal catalyzed reduction of NO by CO was only considered in the reducing zone.

Fig. 12 shows the axial NO profiles through both the reducing and oxidizing zones. The NO concentration profile predicted by the model corresponds qualitatively to those measured on full-scale (Thomsen et al., 1998). Initially, when the fuel is admitted, NH_3 is oxidized rapidly in the presence of char and NO is reduced by CO and char. In the oxidizing zone, when the mixing of oxygen is instantaneous, NO is rapidly formed by char-N oxidation and the concentration increases. Also, at high local oxygen concentration, the combustion rate of char increases, which results in the reduction of char content and the decrease of NO reduction rate. When the oxygen is slow mixed, NO concentration increases slowly due to the low local oxygen concentration in the first part of the reactor (at low oxygen concentration, char content is high and NO reduction rate increases). NO concentration is higher in the case of instantaneous mixing due to the high temperature in the first part of the calciner. The emission of NO depends on temperature because the reaction rates constant of char combustion and nitrogen-related reactions change significantly with the temperature. With the increase of temperature, the char combustion rate increases and NO concentration increases. On the other side, the rate of NO destruction is reduced due to lower char concentration in the calciner and as a result the concentration of NO also increases.

NO formation rate from char-N depends strongly on temperature, oxygen concentration, char properties and mixing of oxygen and nitrogen. The most important reaction for NO production from volatile-N is the catalytic oxidation of ammonia with char as a catalyst. The oxidation of ammonia catalyzed by CaO has less importance for NO formation (the reason is the low NH_3 concentration when CaO is formed). Also, the homogeneous oxidation of ammonia has less importance. About 75% of the volatile-N are oxidized catalytically (by char) to N_2. The most important reactions for NO reduction are the reactions NO + CO (catalyzed by CaO) and NO + char. The reduction of NO by ammonia is not very important, neither in the gas phase, nor catalyzed. One reason is that the NH_3 concentration in the calciner is very low because of the fast heterogeneous oxidation reactions.

4. Conclusions

The development of an in-line low-NO_x calciner heterogeneous model based on a reaction–diffusion approach for char combustion and limestone calcination was presented and discussed. Char and limestone particles were considered non-isothermal, external heat and mass transfer resistances were taken into account and the reactor was considered operated under adiabatic conditions. The gas and solid flow in the two zones of the calciner were described by an axial dispersion model and mixing in the oxidizing zone was modeled using a modified Zwietering approach, which supposes that combustion air is gradually mixed into the main flow.

The results of simulations show that at the particle level, external heat and mass transfer are not limiting, internal diffusion is important especially in the reducing zone and the first part of the oxidizing zone and internal heat transport limitations are significant for limestone calcination.

At the reactor level, the calculations show that both zones of the calciner are dilute systems in the pneumatic transport regime. The rate at which preheated combustion air is mixed into the main flow has a strong effect on combustion and calcination rates, it has some influence on the CO concentration profile and an important influence on the degree of fuel-N to NO conversion.

Notation

a_{ch}	specific internal surface area of char (per unit particle volume), m^2/m^3
a_s	external surface area of the char particle per unit reactor volume, m^2/m^3
a'_s	external surface area of the limestone particle per unit reactor volume, m^2/m^3
c_{pj}	heat capacity of the component j, J/kg K
C_j	concentration of the component j, $kmol/m^3$
C_{ch}	char concentration, kg/m^3
C_c	limestone concentration, kg/m^3
C_{CaCO_3}	$CaCO_3$ concentration, kg/m^3
C_{CaO}	CaO concentration, kg/m^3
C_{D_s}	drag coefficient of particle
d_c	reactor diameter, m
d_p	particle diameter, m
D_j	molecular diffusivity of the component j, m^2/s
D_j^{eff}	effective diffusivity of the component j, m^2/s
D_s	axial dispersion coefficient for the solid phase, m^2/s
D_G	axial dispersion coefficient for gas phase, m^2/s
D_K	Knudsen diffusivity, m^2/s
$D_{V_G}^{oxdn}$	flow rate of combustion air, m^2/s
E	activation energy, J/mol
F_p	pressure gradient due to particle–wall friction, Pa/m
F_G	pressure gradient due to fluid–wall friction, Pa/m
$F_{N,ch}$	molar ratio of nitrogen to carbon remaining in char after devolatilization
g	acceleration due to gravity, m^2/s
G_G	mass flux of gas, kg/m^2 s
G_s	mass flux of solid phase, kg/m^2 s
H	reactor height, m

$(-\Delta H_c)$ heat of the calcination, J/kmol
$(-\Delta H_{\text{gasn}})$ heat of gasification, J/kmol
$(-\Delta H_{\text{oxdn}})$ heat of combustion, J/kmol
$(-\Delta H_{Ri})$ heat of reaction i, J/kmol
k_c calcination rate constant, kmol/m^2 s
k_{CO} rate constant for the homogeneous carbon monoxide oxidation
k_{dest} rate constant for the NO reduction reaction
k_G mass transfer coefficient, m/s
k_{mix} mixing rate constant, 1/s
M_j molar mass, kg/kmol
Nu Nusselt number, dimensionless
q burning rate, kmol/m^2 s
P pressure, Pa
P_j partial pressure of component j, Pa
$P_{\text{CO}_2,e}$ equilibrium CO_2 pressure for $CaCO_3$ decomposition, Pa
Pe_h Peclet number for heat transfer, $Pe_h = \rho_G c_{pG} u_G/\lambda_G$
Pe_s Peclet number for solid phase, $Pe_s = v_s H/D_s$
Pe_G Peclet number for gas phase, $Pe_G = u_G H/D_G \varepsilon_G$
Pr Prandtl number, dimensionless
r radial position in the char and limestone particles, m
r_c calcination rate, kmol/m^2 s
r_{dest} reaction rate per unit particle volume for the NO reduction, kmol/m^3 s
r_{film} reaction rate for the homogeneous carbon monoxide oxidation, kmol/m^3 s
r_{gasn} intrinsic carbon consumption rate with carbon dioxide, kmol/m^3 s
r_i reaction rate per unit volume of reactor, kmol/m^3 s
r_{oxdn} intrinsic carbon consumption rate with oxygen, kmol/m^3 s
r_p char particle radius, m
R gas constant
R_p limestone particle radius, m
Re_p particle Reynolds number, dimensionless
S reactor section, m^2
S_v local specific reaction surface area, m^2/kg
Sc Schmidt number, dimensionless
Sh Sherwood number, dimensionless
$\bar{t}$ mean residence time, s
T temperature, K
u_{ch} velocity of char particle, m/s
u_G superficial gas velocity, m/s
v_c interstitial velocity of limestone particle, m/s
v_{ch} interstitial velocity of char particle, m/s
v_G interstitial gas velocity, m/s
v_s interstitial velocity of solid particle, m/s
x axial film coordinate, m
x_c extent of calcination, dimensionless
x_{ch} carbon conversion
y_j molar fraction of component j
z axial reactor coordinate, m

Greek letters

α, β stoichiometric coefficients
α_G heat transfer coefficient for a sphere, W/m^2 K
β fluid–particle interphase drag coefficient, kg/m^4
δ boundary layer thickness, $\delta = b - r_p$
ε voidage of the bed
ε_c limestone fraction
ε_G gas holdup
ε_p particle porosity
ε_s solid holdup
η effectiveness factor (apparent rate/intrinsic reaction rate without diffusional limitation)
λ thermal conductivity, W/m K
μ_G gas viscosity, kg/m s
$v_{i,j}$ stoichiometric coefficient
ρ density, kg/m^3
ϕ Thiele modulus, $\phi = (d_p/2)(k_1 RT a_{\text{ch}}/D_{\text{O}_2}^{\text{eff}})^{1/2}$
ψ pore structure parameter, dimensionless

Subscripts

c calcination, limestone particle
ch char particle
dest destruction
e equilibrium
form formation
F gas film
gasn gasification
G gas phase
in initial
oxdn oxidation
s particle surface, solid phase

Superscripts

e equilibrium
eff effective
in initial

References

Aarna, I., & Suuberg, E. M. (1997). A review of the kinetics of the nitric oxide–carbon reaction. *Fuel*, *76*, 475–491.

Andersen, P. S. (1981). *Cementfabrikken*. Valby, Copenhagen: F.L. Smidth & Co. A/S.

Baker, E. H. (1962). The calcium oxide–carbon dioxide system in the pressure range 1–300 atmospheres. *Journal of the Chemical Society*, 464–470.

Ballal, G., & Zygourakis, K. (1986). Gasification of coal chars with carbon dioxide and oxygen. *Chemical Engineering Communications*, *49*, 181–190.

Basu, P., & Fraser, S. A. (1991). *Circulating fluidized bed boilers—design and operation*. Boston: Butterworth-Heinemann, (Chapter 4) (pp. 95–126).

Basu, P. (1999). Combustion of coal in circulating fluidized-bed boilers: a review. *Chemical Engineering Science*, *54*, 5547–5557.

Bird, R. B., Stewart, W. E., & Lightfoot, E. N. (1960). *Transport phenomena*. New York: Wiley.

Borgwardt, R. H. (1985). Calcination kinetics and surface area of dispersed limestone particles. *A.I.Ch.E. Journal*, *31*, 103–111.

Bradley, D., Chin, S. B., & Draper, M. S. (1976). Aerodynamic and flame structure within a jet-stirred reactor. *16th symposium* (*international*) *on combustion* (pp. 1571–1581). The Combustion Institute, Pittsburgh.

Broden, H. (1994). *Dynamic single particle char combustion and its influence on the fate of fuel bound nitrogen*. Thesis for the Degree of Licentiate of Engineering, Goteborg.

Chambers, A., Yoshii, Y., Inada, T., & Miyamoto, T. (1996). Ammonia decomposition in coal gasification atmospheres. *Canadian Journal of Chemical Engineering*, *74*, 929–934.

Chan, L. K., Sarofim, A. F., & Beer, J. M. (1983). Kinetics of NO–carbon reaction at fluidized bed combustion conditions. *Combustion and Flame*, *52*, 37–44.

Dernedde, E., Charette, A., Bourgeois, T., & Castonguay, L. (1986). Kinetic phenomena of the volatiles in ring furnaces. *Proceedings of the 115th AIME Annual Meeting – Light Metal*, New Orleans, (pp. 589–592).

Dryer, F. L., & Glassman, I. (1973). High temperature oxidation of CO and CH_4. *14th symposium* (*international*) *on combustion* (pp. 987–592). The Combustion Institute, Pittsburgh.

Duo, W., Dam-Johansen, K., & Ostergaard, K. (1992). Kinetics of the gas-phase reaction between nitric oxide, ammonia and oxygen. *Canadian Journal of Chemical Engineering*, *70*, 1014–1020.

Field, M. A., Gill, D. W., Morgan, B. B., & Hawksley, P. G. (1967). *Combustion of pulverised coal*. Leatherhead: BCURA.

Finlayson, B. A. (1972). *The method of weighted residuals and variational principles*. New York: Academic Press.

Furusawa, T., Tsunoda, M., & Kunii, D. (1982). Nitric oxide reduction by hydrogen and carbon monoxide over char surface. *ACS Symposium Series*, *196*, 347–357.

Furusawa, T., Tsujimura, M., Yasunaga, K., & Kojima, T. (1985). Fate of fuel bound nitrogen within fluidized-bed combustor under staged air firing. *Proceedings of the 8th International Conference on Fluidized Bed Combustion*, Vol. 3 (pp. 1095–1104).

Glarborg, P., Alzueta, M. U., Dam-Johansen, K., & Miller, J. A. (1998). Kinetic modeling of hydrocarbon/nitric oxide interactions in a flow reactor. *Combustion and Flame*, *115*, 1–27.

Greul, U., Rüdiger, H., Spliethoff, H., & Hein, K. R. G. (1993). Untersuchung der brennstoffstufung mit pyrolysegas als reduktionsbrennstoff an einer versuchsanlage. *VDI Berichte*, *1090*, 17–26.

Hautman, D. J., Dryer, F. l., Schug, K. P., & Glassman, I. (1981). *Combustion Science and Technology*, *25*, 219–227.

Hu, N., & Scaroni, A. W. (1996). Calcination of pulverized limestone particles under furnace injection conditions. *Fuel*, *75*, 177–186.

Hundebøl, S., & Kumar, S. (1987). Retention time of particles in calciners of the cement industry. *Zement-Kalk-Gips*, *8*, 422–425.

Jensen, L. S. (1999). NO_x *from cement production—reduction by primary measures*. Ph.D. Thesis, Technical University of Denmark.

Jeschar, R., Jennes, R., Kremer, H., & Kellerhoff, Th. (1996). Optimierung der verbrennung im calcinator einer zementdrehofenanlage. *ZKG-International*, *6*, 304–317.

Jeschar, R., Jennes, R., Kremer, H., & Kellerhoff, Th. (1999). Reduzierung der NO_x- und CO-emissionen durch verbrennung von kunststoffen im calcinator einer zementdrehofenanlage. *ZKG-International*, *10*, 534–549.

Kaviany, M. (1991). *Principles of heat transfer in porous media*. New York: Springer.

Keener, S., & Khang, S.-J. (1992). A structural pore development model for calcination. *Chemical Engineering Communications*, *117*, 279–291.

Khinast, J., Krammer, G. F., Brunner, Ch., & Staudinger, G. (1996). Decomposition of limestone: the influence of CO_2 and particle size on the reaction rate. *Chemical Engineering Science*, *51*, 623–634.

Kulasekaran, S., Linjewile, T. M., Agarwal, P. K., & Biggs, M. J. (1998). Combustion of a porous char particle in an incipiently fluidized bed. *Fuel*, *77*, 1549–1560.

Kulasekaran, S., Linjewile, T. M., & Agarwal, P. K. (1999). Mathematical modeling of fluidized bed combustion 3. Simultaneous combustion of char and combustible gases. *Fuel*, *78*, 403–418.

Laurendeau, N. M. (1978). Heterogeneous kinetics of coal char gasification and combustion. *Progress in Energy Combustion*, *4*, 221–230.

Lewis, P. F., & Simons, G. A. (1979). Char gasification: Part II oxidation results. *Combustion Science and Technology*, *20*, 117–126.

Massman, W. J. (1998). A review of the molecular diffusivities of H_2O, CO_2, CH_4, CO, O_3, SO_2, NH_3, N_2O, NO, and NO_2 in air, O_2, and N_2 near STP. *Atmospheric Environment*, *32*, 1111–1127.

Mitchell, J. W., & Tarbell, J. M. (1982). A kinetic model of nitric oxide formation during pulverized coal combustion. *A.I.Ch.E. Journal*, *28*, 302–311.

Namkung, W., & Kim, S. D. (1998). Gas backmixing in a circulating fluidized bed. *Powder Technology*, *99*, 70–78.

Nieuwland, J. J., Delnoij, E., Kuipers, J. A. M., & van Swaaij, W. P. M. (1997). An engineering model for dilute riser flow. *Powder Technology*, *90*, 115–123.

Rajan, R. R., & Wen, C. Y. (1980). A comprehensive model for fluidized bed coal combustors. *A.I.Ch.E. Journal*, *26*, 642–655.

Rossberg, M. (1956). Experimentelle Ergebnisse uber die Primar-reaktionen bei der Kohlenstoffverbrennung. *Zeitschrift fur Elektrochemie*, *60*, 952–956.

Sahu, R., Levendis, Y. A., Flagan, R. C., & Gavalast, G. R. (1988). Physical properties and oxidation rates of chars from three bituminous coals. *Fuel*, *67*, 275–281.

Saterfield, C. N. (1970). *Mass transfer in heterogeneous catalysis*. Cambridge: MIT Press.

Scheuer, A. (1987). *Theoretische und betriebliche untersuchungen zur bildung und zum abbau von stickstoffmonoxid in zementd-rehofenanlagen*. Dissertation Technische Universitat Clausthal, Schriftenreihe der Zementindustrie, Heft 49.

Song, Y. H., Beer, J. M., & Sarofim, A. F. (1982). Oxidation and devolatilization of nitrogen in coal char. *Combustion Science Technology*, *28*, 177–185.

Thomsen, K., Jensen, L. S., & Schomburg, F. (1998). Inbetriebnahme und betrieb des ILC-LowNOx-calcinator bei Lone Star in St. Cruz, Kalifornien. *ZKG-International*, *10*, 542–550.

Timar, P., & Mierka, O. (1997). Numerical solution of the mathematical model of vertical pneumatic transport and related problems. *Powder Handling and Processing*, *9*, 111–115.

Tsujimura, M., Furusawa, T., & Kunii, D. (1983a). Catalytic reduction of nitric oxide by hydrogen over calcined limestone. *Journal of Chemical Engineering of Japan*, *16*, 524–526.

Tsujimura, M., Furusawa, T., & Kunii, D. (1983b). Catalytic reduction of nitric oxide by carbon monoxide over calcined limestone. *Journal of Chemical Engineering of Japan*, *16*, 132–136.

Van den Bleek, C. M., & Van den Berg, P. J. (1980). The difficulty of reducing nitrogen oxides in the presence of oxygen. *Journal of Chemical Technology and Biotechnology*, *30*, 467–473.

Villadsen, J., & Michelsen, M. L. (1978). *Solution of differential equations models by polynomial approximation*. New York: Prentice-Hall.

Vilienskii, T. V., & Hezmalian, D. M. (1978). Dynamics of the combustion of pulverized fuel. *Energia* (*Moscow*), *11*, 246–251.

Wei, F., Lin, S., & Yang, G. (1993). Gas and solids mixing in a commercial FCC regenerator. *Chemical Engineering and Technology*, *16*, 109–113.

Wei, F., & Zhu, J.-X. (1996). Effect of flow direction on axial solid dispersion in gas–solids concurrent upflow and downflow systems. *Chemical Engineering Journal*, *64*, 345–352.